# Design and evaluation of a bilateral semi-rigid exoskeleton to assist hip motion

Arash Mohammadzadeh Gonabadi <sup>1,2\*</sup>, Prokopios Antonellis <sup>1,3</sup>, Alex C. Dzewaltowski <sup>1,4</sup>, Sara A. Myers <sup>1,6</sup>, Iraklis I. Pipinos <sup>5,6</sup>, Philippe Malcolm <sup>1</sup>

- Department of Biomechanics and Center for Research in Human Movement Variability, University of Nebraska at Omaha, Omaha, NE 68182, USA
- Institute for Rehabilitation Science and Engineering, Madonna Rehabilitation Hospitals, Lincoln, NE 68506, USA
- Department of Neurology, Oregon Health & Science University, Portland, OR 97239, USA
- Scholl College of Podiatric Medicine, Rosalind Franklin University of Medicine & Science, North Chicago, IL 60064, USA
- Department of Surgery, University of Nebraska Medical Center, Omaha, NE 68105, USA
- Department of Surgery and Research Service, Nebraska-Western Iowa Veterans Affairs Medical Center, Omaha, NE 68105, USA
- \* Correspondence: amgonabadi@unomaha.edu; agonabadi@madonna.org

**Abstract:** This research focused on designing and evaluating a bilateral semi-rigid hip exoskeleton. The exoskeleton assisted the hip joint, capitalizing on its proximity to the body's center of mass. Unlike rigid counterparts, the semi-rigid design permitted greater freedom of movement. A temporal force-tracking controller allowed us to prescribe torque profiles during walking. We ensured high accuracy by tuning control parameters and series elasticity. The evaluation involved experiments with ten participants across ten force profile conditions with different end-timings and peak magnitudes. Our findings revealed a trend of greater reductions in metabolic cost with assistance provided at later timings in stride and at greater magnitudes. Compared to walking with the exoskeleton powered off, the largest reduction in metabolic cost was 9.1% when providing assistance using an end-timing at 44.6% of the stride cycle and a peak magnitude of 0.11 Nm kg-1. None of the tested conditions reduced the metabolic cost compared to walking without the exoskeleton, highlighting the necessity for further enhancements, such as a lighter and more form-fitting design. Interestingly, the optimal end-timing paralleled findings from a soft hip exosuit study, suggesting a similar interaction with this prototype compared to entirely soft exosuit prototypes.

**Keywords:** Exosuit; Force-tracking; Metabolic cost; Actuation magnitude; Timing; Walking; Biomechanics; Robotics; Biomedical Engineering

#### 1. Introduction

While the primary focus in the development of exoskeletons targeting metabolic cost reduction has been directed towards aiding the ankle joint [1–3], there is potential for greater reductions by assisting other joints than the ankle. Research has shown that the hip joint contributes up to 45% of the mechanical power during walking [4], leading to a growing interest in extending assistance to the hip joint [5–

7]. The distinctive muscle characteristics and less prominent presence of efficient elastic tendons in hip joint muscles could cause the hip to consume more energy compared to the ankle, which has more efficient en-

ergy storage and return from the Achilles tendon [4,8,9]. Despite this, reductions achieved by assisting the hip joint still appear lower than those achieved with ankle exoskeletons [10–14]. More research is needed to better understand the relationships between energetic benefits and assistance levels at the hip [6,15–17].

Assisting at the hip has the added advantage of positioning the device closer to the body's center of mass, thereby minimizing the added mass penalty [18]. Experimental studies and simulations also reveal that exoskeletons can assist muscles from multiple joints, even those they do not directly cover [19]. For example, an ankle exoskeleton can indirectly assist the hip [20]. This capability to assist multiple joints offers an exciting opportunity to combine the advantages of minimizing the mass penalty and providing assistance at the hip. Such a combination can be particularly beneficial in patient populations prone to ulcer formation at the feet. Approximately 40% of the metabolic cost during level walking is attributed to the hip muscles [21–23]. Thus, various groups have developed both rigid exoskeletons and soft exosuits to assist the hip [6,9,24–26]. Soft exosuits, in particular, allow for greater freedom of movement [6]. However, they often cannot apply the same torque magnitudes as rigid exoskeletons and must rely on skin friction to remain anchored [25].

Both rigid and soft exoskeletons present their respective merits and challenges. While rigid exoskeletons enable the generation of controllable and accurate assistive torques, they are more complex and heavier due to misalignment issues [27]. In contrast, soft exoskeletons can address this misalignment problem because of their elasticity, yet still require skin friction for anchoring, potentially causing discomfort [27]. Recently, there has been a shift towards developing semi-rigid exoskeletons that merge the beneficial characteristics of both rigid and soft exoskeletons. Zhang et al. [27] introduced a semi-rigid knee exoskeleton to minimize misalignment while retaining some aspects of both designs. Schmidt et al. [28] developed a Myosuit to provide continuous assistance at the hip and knee joints when working with and against gravity in activities of daily living. Lin et al. [29] also accomplished a compliant and accurate model in their innovative soft-rigid hand exoskeleton. Developing semi-rigid exoskeletons to become more mechanically efficient is an essential topic of ongoing research.

Here, we detail the development of a bilateral semi-rigid hip exoskeleton end-effector to assist hip extension during walking. Our semi-rigid design allows for more freedom of movement than a traditional hinged hip exoskeleton. The aim of our study was to optimize the mechanical components and the controller settings to maximize force-tracking performance, hypothesizing that a specific series of elastic stiffness and controller gain settings will maximize accuracy. We also investigated the effect of one assistance timing and one assistance magnitude parameter on metabolic cost. We hypothesized the timing of peak assistance would affect metabolic cost following a U-shaped trend versus timing. We also hypothesized that increasing magnitudes of assistance would monotonically reduce metabolic cost

#### 2. Materials and Methods

# 2.1. Hip Exoskeleton Design

We developed a semi-rigid hip exoskeleton end-effector intended to allow more freedom of movement than a hinged hip exoskeleton while improving anchoring to the body segments (Figure 1). The waist-belt and thigh segments are rigid but not connected via hinges. The hip exoskeleton is linked to a commercially high-powered, off-board actuation system (HuMoTech, Pittsburgh, PA), applying forces to the dorsal side of the hip to assist in hip extension. On the frontal side of the hip, a set of springs provides passive hip flexion assistance. Safety features include a remote stop button, a software force limit (software fuse) to stop the motor if load cell force exceeds 300 N, and a mechanical fuse consisting of a thin piece of rope that disconnects if the tension exceeds its breaking strength.

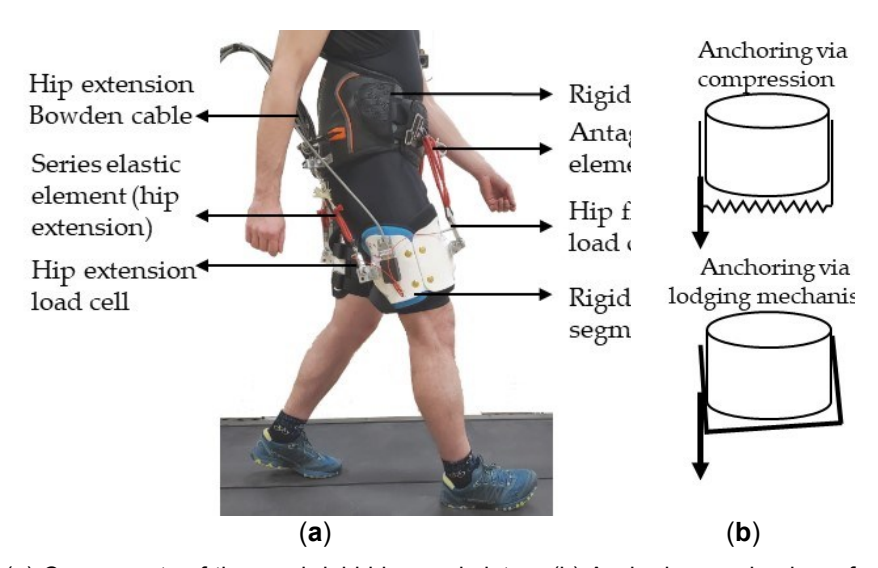


**Figure 1. Exoskeleton Design**. (a) Components of the semi-rigid hip exoskeleton. (b) Anchoring mechanism of the semi-rigid exoskeleton. The exoskeleton anchors to the waist through a combination of compression forces and a mechanism in which the waist belt becomes lodged when the actuation force attempts to rotate the waist belt.

# 2.2. Exoskeleton Controller

We developed a high-level temporal controller that allows the independent application of sinusoidal extension and flexion torque profiles to each leg as a function of the stride cycle percentage (Figure 2). We measured the ground reaction forces of both legs at 1000 frames per second using a split-belt force treadmill (Bertec, Columbus, OH) and estimated the percentage of stride time based on the most recent heel contact time and a moving average of previous steps. The controller calculated the forces needed to achieve a specific net torque during hip extension, given forces generated by the hip flexion springs and a torque arm assumed to be 10 cm. The error between the actual forces, measured with the load

cell, and the desired forces was minimized using a low-level controller developed by HuMoTech, which employs a closed-loop proportional-integral—derivative (PID) algorithm with configurable gains [30]. A control station comprising an input-output interface (HuMoTech) and a real-time computer (SpeedGoat, Liebefeld, Switzerland), runs the controller in Simulink (MathWorks).

We selected the general shape of the actuation profile based on a review of force profiles in the literature [6,9,24–26]. Considering the limits of the forces we could achieve, we chose to model the force profile after the one used by Lee et al. [24], which resulted in a substantial 21% reduction in metabolic cost with a relatively low peak moment of around 7.5 Nm. Inspired by the optimal torque profile in that study, we set the desired onset of the extension torque at 90% of the stride with a peak extension torque timing at 17% of the stride cycle. Under different conditions, we varied the end timing of the extension torque and peak magnitude.

## 2.3. Exoskeleton Design and Control Optimization Protocol

We conducted several single-subject analyses, including optimization of the stiffness of the series elastic element of the hip extension actuation and the gains of the PID controller, to determine the optimal device and control parameters. Torque tracking was assessed by calculating the root-mean-square error (RMSE) between the actual and desired torque. We measured how well the system tracked the torque profiles within each stride by calculating the RMSE for each stride's actual and desired torque time series. Additionally, we reported the RMSE of the average torque per step to gauge how well the system tracked the average torque per stride [31,32]. We employed an oscillation-level metric proposed by Zhang et al. (Zhang et al. 2017) to detect unwanted high-frequency oscillations. This metric is obtained by high-pass filtering the error with a 10Hz cut-off frequency and then integrating the energy spectral density. All analyses were performed in MATLAB (MathWorks, Natick, MA).

# Low-level control

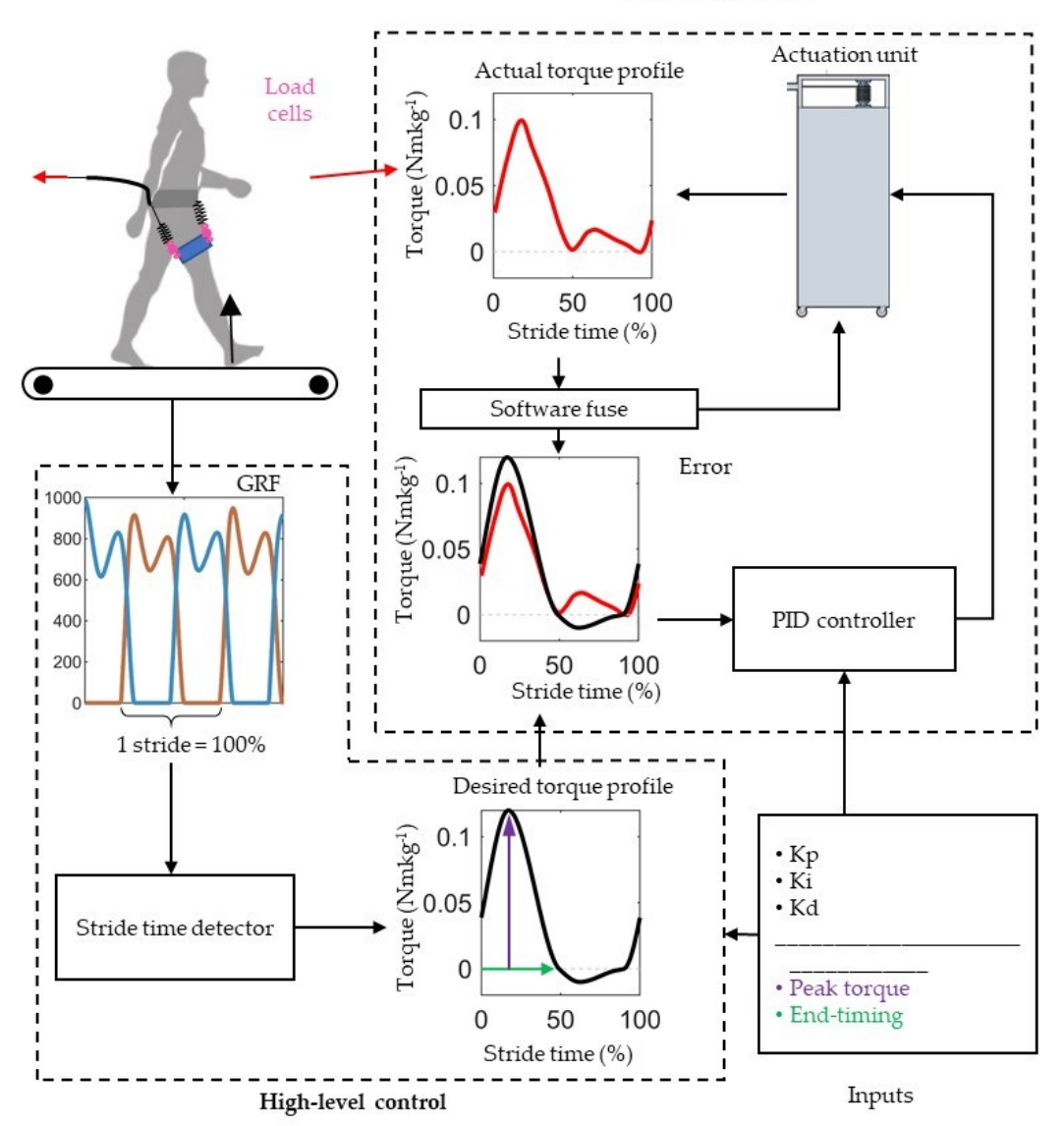


**Figure 2. Control Algorithm Overview.** This figure illustrates the high-level control strategy, where the controller sets desired torque profiles based on stride time. The profiles indicate the target torque that the controller aims to provide, not the actual measured output torque of the hip joint. A low-level PID controller is then employed to adjust the motor velocity, ensuring precise adherence of the actual torque measured by the load cell to these target profiles throughout the stride.

### 2.4. Metabolic Cost and Biomechanics Evaluation Protocol

Ten healthy adults (4 males, 6 females, age:  $27.6 \pm 5.9$  years, body mass:  $65.3 \pm 13.1$  kg, height:  $1.66 \pm 0.08$  m) participated in this study. The testing session started with a five-minute standing trial to measure the resting metabolic rate and was followed by a warm-up of approximately 20 minutes. During this warm-up, we cycled through all the force profile conditions and adjusted the gain tuning settings for individuals if needed. During the testing protocol, we maintained the onset and peak of the extension torque constant while varying the end-timing and peak magnitude across ten different conditions. These conditions included combinations of five distinct desired end-timings, ranging from 21% to 49%, and two desired peak torque magnitudes, ranging from 0.06 to 0.12 Nm kg-1 (Figure 3). In addition to these ten conditions, participants also walked in two reference conditions: one without actuation (Power-Off) and another without wearing the exoskeleton (No-Exo). The entire protocol was split into three blocks in which conditions were completed back-to-back. Each block had low and high magnitudes and different timings presented in random order. The first and last condition of each block lasted 5 minutes. All the other trials lasted 2 minutes. Between the blocks, participants rested for at least 10 minutes.

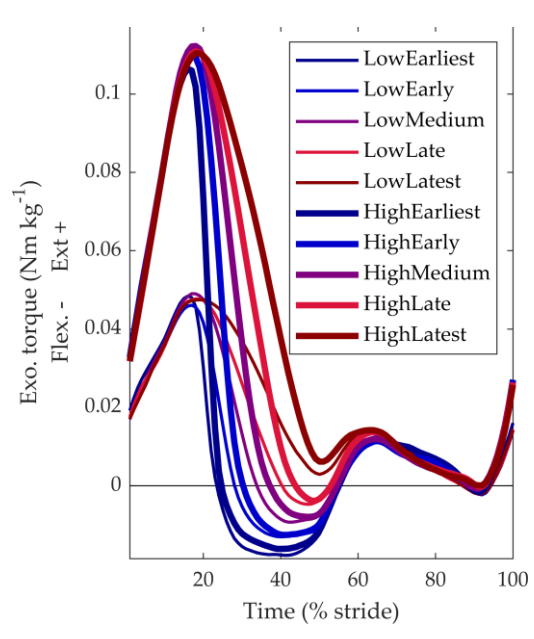


Figure 3. Actuation profiles. The ten actuation profiles were used in the metabolic cost and biomechanics evaluation protocol.

We measured oxygen consumption and carbon dioxide production using indirect calorimetry (K5, Cosmed, Rome, Italy). By applying the Brockway equation [33], we converted the breath-by-breath measurements to watts per kilogram (W kg<sup>-1</sup>). We averaged the breath-by-breath data in the final two minutes to estimate the steady-state metabolic rate of the resting trial and the conditions at the beginning of each block. We estimated the steady-state metabolic rates for conditions that only lasted 2 minutes by fitting the breath-by-breath data immediately after transitioning to each new condition until just before the change to the next condition with an exponential function and estimating the asymptote [34,35]. We calculated the net metabolic rate of walking by subtracting the metabolic rate of standing at rest from the metabolic rate under each walking condition.

We also recorded 3D kinematics using motion capture (VICON Vero, Oxford Metrics, Yarnton, U.K.; 2000 Hz) from 23 reflective markers placed on anatomical landmarks on the skin, tight-fitting suit, or the exterior of the shoes according to a modified Helen Hayes marker set [36]. Kinematic data were tracked from each condition in Nexus software (Vicon Motion Systems Inc., Oxford, United Kingdom) and exported as a Visual 3D file (Visual 3D, C-Motion, Germantown, MD) for further processing. We filtered the ground reaction forces with a low-pass Butterworth filter with a 6 Hz cut-off and processed motion capture data using OpenSim (version 4.0, SimTK, Santa Clara County, California; [37,38]) with the model from Rajagopal et al., [37,39]. After scaling the model based on motion capture data from a static pose with the "adjust model markers" and "preserve mass distribution" options, we adjusted the calculated mass distribution to account for the exoskeleton's mass (5.77 kg). We used the inverse kinematics tool to estimate joint kinematics from the marker data, restricting the ankle and knee motion to one degree of freedom (flexion and extension) but utilizing all three degrees of freedom for the hip to simulate walking's hip movement realistically. We applied the inverse dynamics tool with a 6 Hz cut-off filter setting for marker coordinates to compute joint moments.

To calculate the exoskeleton's applied torque on the hip joint, we measured the force of each sensor on the exoskeleton and multiplied this by the lever arm versus the hip. We assumed a fixed value (10 cm) for the lever arm. The multiplication of the force and lever arm yielded the applied torque on the hip joint. To calculate the biological moment for the hip, we subtracted the exoskeletal torque from the total moment while reporting the total external moments for the ankle and knee. In addition to investigating the effects on the hip, knee, and ankle moments and powers, we also investigated the effects on the total leg power based on the multiplication of center of mass velocity and ground reaction force using the methods from Donelan and Kuo [40]. In this analysis, we looked at the effects of the different negative and positive work bursts that occur throughout the stride: collision, rebound, preload, and pushoff.

Finally, we analyzed the processed data in MATLAB (MathWorks, Natick, MA). We segmented all data into strides that began at the ipsilateral heel strike and ended with the next ipsilateral heel strike based on foot contact detection from ground reaction force data. Outliers were detected by examining how well signals remained within a band defined by the median plus-minus 1.5 times the interquartile range and removed outlying strides [41].

## 2.5. Statistical Analyses

All metabolic cost and biomechanical variables were analyzed by reporting means and standard error across participants for each condition. We conducted a linear mixed-effects model analysis to examine the effects and interactions of the timing and magnitude of torque profiles on the metabolic rate and biomechanical variables (Equation 1). In this analysis, the participants were considered to be the random factor. Since there were only two magnitude settings, we evaluated only a linear effect of magnitude in the equation. We considered a second-order effect for timing, hypothesizing a U-shaped trend in metabolic cost versus timing. We also multiplied both timing terms by magnitude because the effect of timing could not exist without actuation magnitude. Additionally, we included a constant offset term, resulting in the following regression equation:

Mag × 
$$(c_1 \times Tim^2 + c_2 \times Tim) + c_3 \times Mag + c_4$$

In this equation, 'Tim' and 'Mag' symbolize the desired end-timing and peak torque magnitude. We started with this initial model and removed non-significant terms stepwise until only significant terms remained. To compare the differences between the Power-On conditions versus the Power-Off and No-Exo conditions, we conducted paired t-tests. We performed all statistical analyses in MATLAB (Math-Works, Natick, MA, USA) and set the significance threshold at 0.05.

#### 3. Results

#### 3.1. Device Optimization Results

It is known that series elasticity can influence actuator control performance, with high stiffness offering quicker response times but possibly more noise and low stiffness potentially enhancing force tracking but causing a delay [42–44]. To find the optimal stiffness for the spring in series with the hip extension actuation, we tested nine different springs ranging from 892 to 30'000 Nm<sup>-1</sup>. We examined the effects on within-stride RMSE, between-stride RMSE, and oscillation level, using effective stiffness measured by plotting force change against length change as an independent parameter. The results did not reveal a clear single trend, possibly due to varying spring designs from different suppliers. Nevertheless, a stiffness of 4438 Nm<sup>-1</sup> was generally found to strike the best balance between the difference error metrics, and this value was used in subsequent tests.

Next, we performed a series of experiments to investigate the optimal settings for the three force-tracking parameters: the proportional gain (Kp), which modifies the actuator control signal in relation to the error; the integral gain (Ki), which adjusts the control signal based on the accumulated integral of the error, and the derivative gain (Kd), which adjusts the control signal based on the derivative for the error. First, we varied Kp from 10 to 110, holding Ki and Kd at 0. Based on this experiment, we identified the optimal Kp to be at 95 (Figure 5). Next, we changed Ki from 0 to 0.025, keeping Kp at its optimized setting and Kd at 0. Based on this second sweep, we identified that the optimal Ki was at 0 (Figure 4). Finally, we evaluated the effect of changing Kd from 0 to 0.2 while keeping Kp at 95 and Ki at zero. This test did not show a clear effect of Kd; hence, we kept Kd at zero for future tests. It could be possible that the fact that Kd and Ki did not have a clear effect is due to the fact that the optimized spring already improves the force tracking.

The optimized settings produced a within-stride RMSE of 1.06 Nm, a between-stride RMSE of 0.008 Nm, and an oscillation level of 0.014. In the further metabolic cost and biomechanical parameter evaluations, we only slightly adjusted Kp depending on the participant but kept Ki and Kd at zero.

11

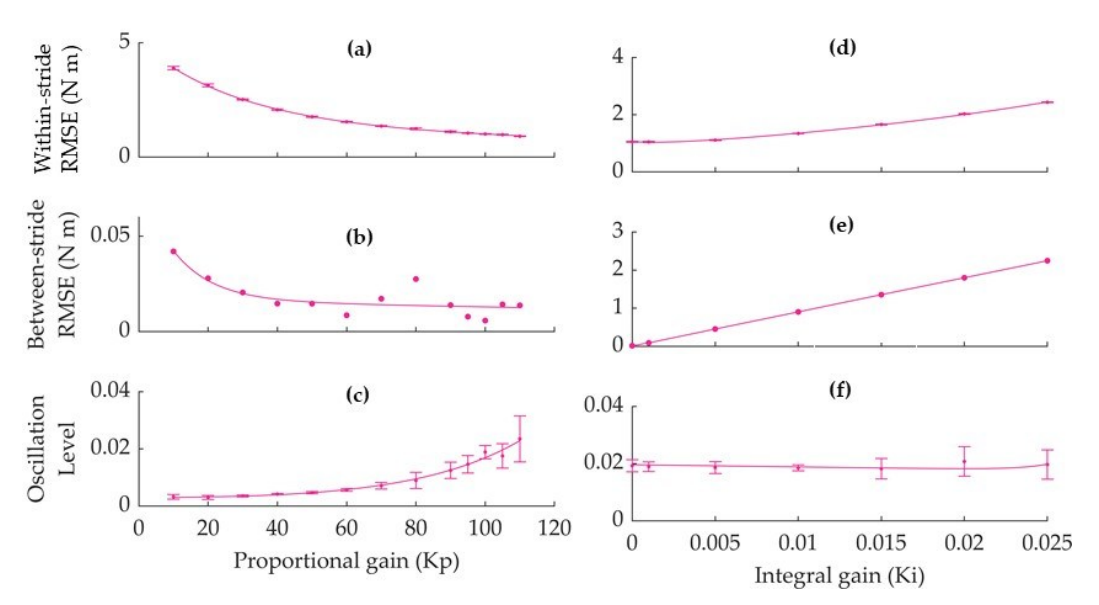


**Figure 4. Gain tuning results.** (a), (b), and (c) Effects of tuning proportional gain (Kp) on within-stride RSME, between-stride RMSE, and oscillation level. (d), (e), and (f) Effects of tuning integral gain (Ki) on within-stride RSME, between-stride RMSE, and oscillation level. Based on these tests, in further experiments, Kp and Ki were set to 95 and 0, respectively.

# 3.2. Metabolic Cost and Biomechanics Evaluation Protocol Results

The programmed desired actuation profile conditions resulted in actual end-timings ranging from 24.8  $\pm$  1.3 % of the stride (mean  $\pm$  S.D. of all early conditions) in the earliest condition to 49.6  $\pm$  1.1 % in the latest condition. The peak magnitudes ranged from 0.0479  $\pm$  0.0084 Nm kg<sup>-1</sup> in the low magnitude conditions to 0.1102  $\pm$  0.0163 Nm kg<sup>-1</sup> in the high magnitude conditions.

According to the following equation, we observed a significant effect of timing and magnitude on the change in metabolic rate versus the no-assist condition (Figure 5).

The interaction term p was the only one required to fit the data (p-value of interaction term:  $p_{\text{Mag} \times \text{Tim}} = 9 \times 10^{-4}$ ) significantly. The other terms from the initial model (*Equation 1*) were insignificant and removed during the stepwise elimination. The trend shows that conditions with greater peak torques and later end-timing produced a greater reduction in metabolic rate. The largest decrease in metabolic rate was  $9.1 \pm 12.5$ % (mean  $\pm$  S.D., p = 0.047, paired t-test between Power-On and Power-Off conditions). This reduction occurred in the highest assistance magnitude and the second latest end-timing. None of the conditions reduced metabolic rate compared to the No-Exo condition. The metabolic rate in the No-Exo condition was 4.8% lower than in the best assistance condition.

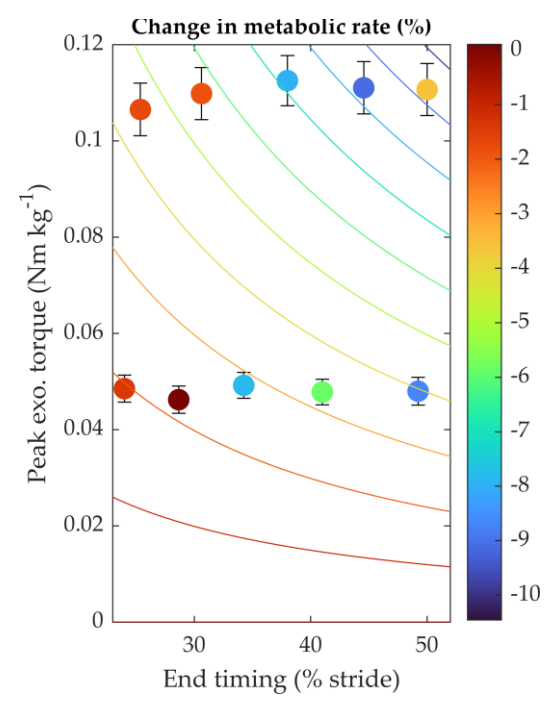


**Figure 5.** Effect of timing and magnitude on change in metabolic rate. Colored dots represent ten conditions. Change in metabolic rate versus no-assist condition is characterized by color scale. End-timings are shown on the horizontal axis, and peak assistance magnitude is shown on the vertical axis. Colored contour lines visualize a trend from a linear mixed-effects model fitted to the data (Change in metabolic rate (%) ~ -1.68 × Mag (Nm kg<sup>-1</sup>) × Tim (%)).

We also observed significant interactions of timing and magnitude on the mean biological hip extension moment, preload work rate, and push-off work rate:

$$(p_{\text{Mag} \times \text{Tim}} = 0.006 \text{ and } p_{\text{intercept}} = 3 \times 10^{-37})$$

$$\text{Preload work rate (W kg}^{-1}) \sim$$

$$0.001 \times \text{Mag (Nm kg}^{-1}) \times \text{Tim}^{2} (\%) - 1.759 \qquad (4)$$

$$(p_{\text{Mag} \times \text{Tim}^{2}} = 0.045 \text{ and } p_{\text{intercept}} = 2 \times 10^{-24})$$

$$\text{Push-off work rate (W kg}^{-1}) \sim$$

$$-0.114 \times \text{Mag (Nm kg}^{-1}) \times \text{Tim (\%)} + 3.470 \times \text{Mag (Nm kg}^{-1}) + 1.873 \qquad (5)$$

$$(p_{\text{Mag} \times \text{Tim}} = 3 \times 10^{-4}, p_{\text{Mag}} = 0.013 \text{ and } p_{\text{intercept}} = 2 \times 10^{-31})$$

Mean biological hip extension moment (Nm kg<sup>-1</sup>)  $\sim$  -0.011 × Mag (Nm kg<sup>-1</sup>) × Tim (%) + 0.361

(3)

For each of these three biomechanical variables, the trends were such that later end-timings and greater assistance magnitude resulted in smaller peak torques and powers. There were no other significant effects on ankle or knee torques and powers.

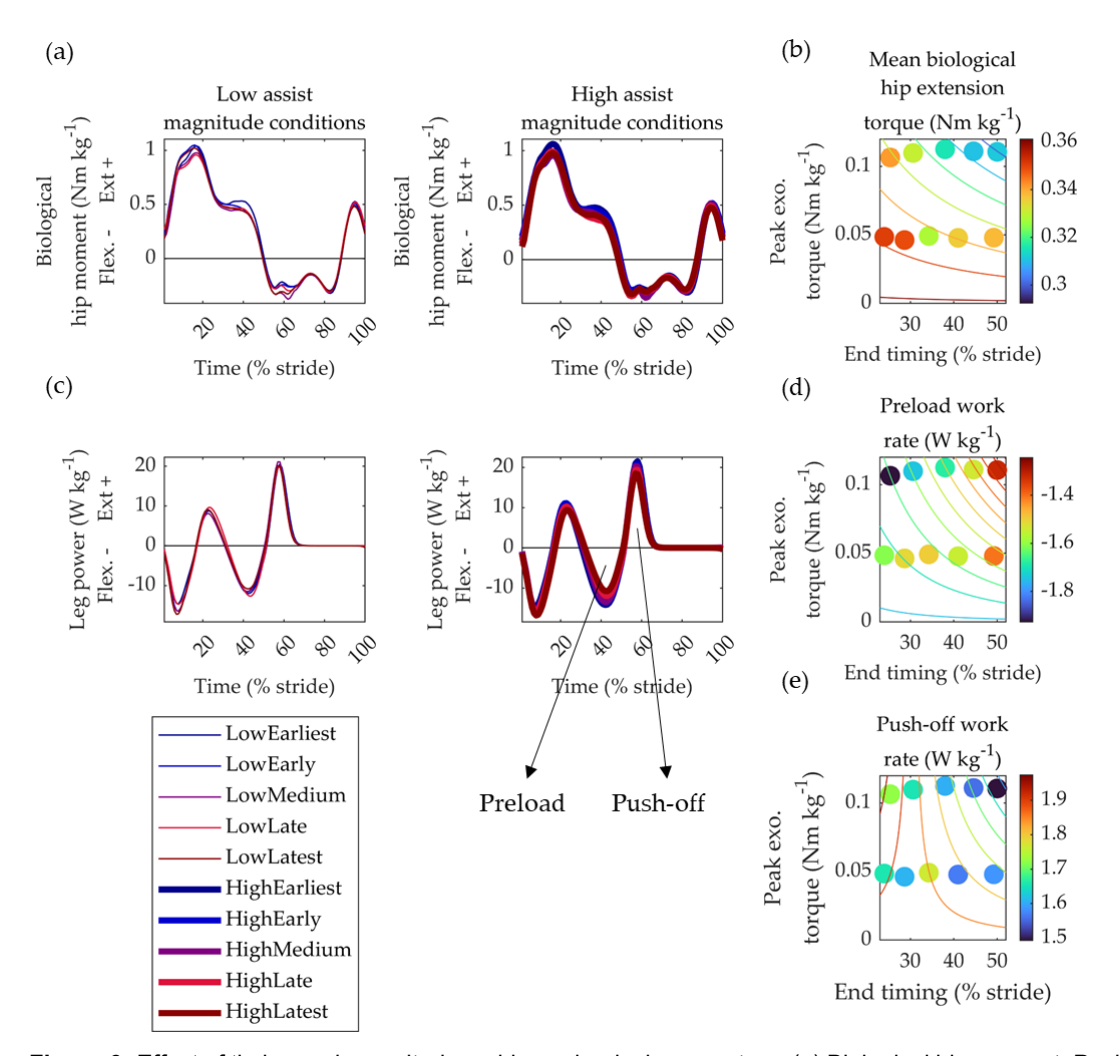


**Figure 6.** Effect of timing and magnitude on biomechanical parameters. (a) Biological hip moment. Positive values represent extension moments, and colored lines in the left figure represent the different timings with low assistance magnitude. Colored lines in the right figure represent different timings with high assistance magnitude. (a) Effect of timing and magnitude on the mean positive biological hip extension moment from panel a. (c) Leg power calculated using the individual limb method. Arrows indicate the different work bursts that showed significant effects in panels d and E. (d) Preload work rate from panel c. (e) Push-off work rate from panel c.

# 4. Discussion

Our study describes the design and evaluation of a semi-rigid hip exoskeleton. In the first part of the manuscript, we explain how optimizing the proportional gain reduced the within-stride RMSE to about 1 Nm. In the second part, we describe how human experiments with the optimized exoskeleton show that, compared to the Power-Off condition, the greatest reduction of 9.1% was found in the condition with the greatest peak torque and the second-latest end-timing. We found an interaction of magnitude but no isolated effects of timing or magnitude. Furthermore, none of the conditions reduced metabolic rate compared to the No-Exo condition.

It was surprising that we did not find a clear trend showing optimal stiffness or derivative gain's effect with this exoskeleton. This contrasts with experiments involving other types of wearable robots, such as ankle exoskeletons or a robotic waist tether, which show the presence of an optimal series elastic stiffness that improves force tracking [32,45]. Regarding the investigation of the effect of stiffness, it is important to note that we used a range of coil springs with different dimensions and masses to cover the sweep range (McMaster-Carr, Elmhurst, IL, USA). These diverse material properties may affect the RMSE in various ways; for instance, springs with a heavier mass might oscillate differently. This variability could have contributed to the inability to observe a clear trend.

The achieved optimal RMSE was approximately 1 Nm, constituting around 35.5% of the peak torque in magnitude conditions and 15.2% in high-magnitude conditions. This substantial variability is likely attributed to the inherent challenges associated with a semi-rigid design, such as the movement of components on the participant. This variability may explain the relatively large fluctuations observed in metabolic effects. Our metabolic cost and biomechanical evaluation protocol identified a trend indicating a greater reduction with later end-timing and increased assistance magnitude. Other biomechanical

parameters exhibiting significant trends in relation to timing and magnitude help elucidate why later timing and magnitude contributed to a reduction in metabolic cost. As anticipated, we observed that the timing and magnitude that reduced metabolic cost also decreased the biological component of the hip extension moment. The greater reduction observed with increased magnitude and later end-timing is likely due to the exoskeleton torque more effectively covering a larger portion of the extension burst in the total hip moment.

More surprising were the reductions in leg power during the preload and push-off phases, where the push-off phase primarily relies on ankle push-off from the center-of-mass power. It is established that walking with a more intensive hip extension diminishes the need for push-offs and vice versa [46]. Hence, the hip exoskeleton's greater magnitude and later-end timing may increase total hip extension and reduce the push-off requirement. The finding that later end-timing reduces metabolic rate aligns with results from studies on other hip assistance devices. Ding et al. utilized a human-in-the-loop approach to optimize peak timing and end-timing, discovering that optimal conditions often featured an end-timing close to the maximal range set for the experiment [47]. In both our study and theirs, the optimal end-timing was later than when the biological hip extension moment ended. This highlights that the optimal assistance pattern does not necessarily mirror physical kinetics [48].

Limitations of the study include the relatively high variability in the actual actuation patterns and their effects on metabolic cost. Due to this variability, no conditions were found to significantly reduce the metabolic rate compared to walking without the exoskeleton. In the No-Exo condition, the metabolic cost was approximately 4.8% lower than in the best assistance condition. Considering that the exoskeleton mass of 5.77 kg is primarily situated around the waist, and each additional kilogram results in roughly a 1% increase in metabolic cost [18], theoretically reducing the exoskeleton mass could bring the cost of the best assistance condition close to walking without the exoskeleton. It is possible that the exoskeleton would work better in populations who have a more impaired gait; however, this is unknown at this point, and it is also possible that the exoskeleton would be less effective in such populations. To achieve greater reductions in metabolic cost, it will likely be necessary further to enhance the fit and comfort of the exoskeleton design and optimize other parameters of the actuation pattern (e.g., onset time, peak time, peak magnitude), as studies have shown that these parameters all impact metabolic cost [49]. Optimizing multiple parameters simultaneously could be achieved through human-in-the-loop optimization. Our group is currently working developing lighter and simpler passive-elastic exoskeletons to address this limitation. Additionally, as highlighted in previous research, users' adaptation to the exoskeleton is crucial for optimizing its effectiveness [50]. In the present study, participants only walked for approximately 4 minutes in each condition. It is possible that longer habituation, potentially involving multiple sessions, could have influenced the results..

#### 5. Conclusion

The present study demonstrates the effects of a semi-rigid design in assisting walking, making progress compared to previous efforts with semi-rigid designs that predominantly focused on static activities, such as sit-to-stand transitions. Our findings revealed a trend of greater reductions in metabolic cost with later timings and greater magnitudes. In comparison to walking with the exoskeleton powered off, the largest reduction, 9.1%, was observed with an end-timing at 44.6% of the stride cycle and a peak magnitude of 0.11 Nm kg<sup>-1</sup>. None of the tested conditions reduced the metabolic cost below that of walking without the exoskeleton. To achieve more substantial reductions in metabolic cost, further refinement of the exoskeleton design and optimization of other aspects of the actuation pattern will be necessary.

**Supplementary Materials:** The following supporting information can be downloaded at: ..., Data D1: MATLAB source data of Metabolic cost and Biomechanics evaluation protocol.

**Author Contributions:** Conceptualization A.M.G., S.A.M, I.I.P, P.M.; Methodology A.M.G., P.A., A.C.D.; Software A.M.G.; Validation A.M.G.; Formal analysis A.M.G.; Investigation A.M.G., P.A., A.C.D.; Resources S.A.M, I.I.P; Data curation P.M.; Writing - original draft preparation A.M.G., P.M.; Writing - review and editing A.M.G., P.A., A.C.D., S.A.M, I.I.P, P.M.; Visualization A.M.G., P.M.; Supervision P.M.; Project administration A.M.G., P.M.; Funding acquisition S.A.M, I.I.P, P.M..

#### Fundina:

This research was funded by the National Institutes of Health (P20GM109090 to P.M, R01HD090333 to S.A.M, and R01AG0778031 and R01AG062198 to I.I.P), National Science Foundation (2203143 to P.M.) and the U.S. Department of Veterans Affairs Rehabilitation Research and Development Service (I01RX000604 and I01RX003266 to S.A.M). The content is solely the authors' responsibility and does not necessarily represent the official views of the National Institutes of Health or National Science Foundation.

**Institutional Review Board Statement:** The study was conducted in accordance with the Common Rule and approved by the University of Nebraska Medical Center Institutional Review Board (protocol number: 0101-19-FB; initial approval: 04/22/2019).

Data Availability Statement: The data presented in this study are publicly available in supplementary data file S1.

**Acknowledgments:** We would like to thank HuMoTech and the Department of Biomechanics Movement Analysis Core for their technical support.

Conflicts of Interest: The authors declare no conflict of interest.

### References

- 1. Mooney, L.M.; Rouse, E.J.; Herr, H.M. Autonomous Exoskeleton Reduces Metabolic Cost of Human Walking during Load Carriage. *J. Neuroeng. Rehabil.* 2014, *11*, 80, doi:10.1186/1743-0003-11-80.
- 2. Collins, S.H.; Bruce Wiggin, M.; Sawicki, G.S. Reducing the Energy Cost of Human Walking Using an Unpowered Exoskeleton. *Nature* 2015, *522*, 212–215, doi:10.1038/nature14288.
- 3. Malcolm, P.; Quesada, R.E.; Caputo, J.M.; Collins, S.H. The Influence of Push-off Timing in a Robotic Ankle-Foot Prosthesis on the Energetics and Mechanics of Walking. *J. Neuroeng. Rehabil.* 2015, *12*, 21, doi:10.1186/s12984-015-0014-8.
- 4. Sawicki, G.S.; Ferris, D.P. A Pneumatically Powered Knee-Ankle-Foot Orthosis (KAFO) with Myoelectric Activation and Inhibition. *J Neuroeng Rehabil* 2009, 6, doi:10.1186/1743-0003-6-23.
- 5. Young, A.J.; Foss, J.; Gannon, H.; Ferris, D.P. Influence of Power Delivery Timing on the Energetics and Biomechanics of Humans Wearing a Hip Exoskeleton. *Front. Bioeng. Biotechnol.* 2017, *5*, 1–11, doi:10.3389/fbioe.2017.00004.
- 6. Ding, Y.; Kim, M.; Kuindersma, S.; Walsh, C.J. Human-in-the-Loop Optimization of Hip Assistance with a Soft Exosuit during Walking. *Sci. Robot.* 2018, *3*, doi:10.1126/scirobotics.aar5438.
- 7. Lee, G.; Kim, J.; Panizzolo, F.A.; Zhou, Y.M.; Baker, L.M.; Galiana, I.; Malcolm, P.; Walsh, C.J. Reducing the Metabolic Cost of Running with a Tethered Soft Exosuit. *Sci. Robot* 2017, 2, 6708–6731, doi:10.1126/scirobotics.aan6708.
- 8. Umberger, B.R. Stance and Swing Phase Costs in Human Walking. J. R. Soc. Interface 2010, 7, 1329–1340.
- 9. Kang, I.; Hsu, H.; Young, A. The Effect of Hip Assistance Levels on Human Energetic Cost Using Robotic Hip Exoskeletons. *IEEE Robot. Autom. Lett.* 2019, *4*, 430–437, doi:10.1109/lra.2019.2890896.
- 10. Bryan, G.M.; Franks, P.W.; Song, S.; Voloshina, A.S.; Reyes, R.; O'Donovan, M.P.; Gregorczyk, K.N.; Collins, S.H. Optimized Hip-Knee-Ankle Exoskeleton Assistance at a Range of Walking Speeds. *J. Neuroeng. Rehabil.* 2021, *18*, 152, doi:10.1186/s12984-021-00943-y.
- 11. Lim, B.; Lee, J.; Jang, J.; Kim, K.; Park, Y.J.; Seo, K.; Shim, Y. Delayed Output Feedback Control for Gait Assistance With a Robotic Hip Exoskeleton. *IEEE Trans. Robot.* 2019, 35, 1055–1062, doi:10.1109/TRO.2019.2913318.
- 12. Slade, P.; Kochenderfer, M.J.; Delp, S.L.; Collins, S.H. Personalizing Exoskeleton Assistance While Walking in the Real World. *Nat.* 2022 6107931 2022, 610, 277–282, doi:10.1038/s41586-022-05191-1.
- 13. Yandell, M.B.; Tacca, J.R.; Zelik, K.E. Design of a Low Profile, Unpowered Ankle Exoskeleton That Fits Under Clothes: Overcoming Practical Barriers to Widespread Societal Adoption. *IEEE Trans. Neural Syst. Rehabil. Eng.* 2019, 27, 712–723, doi:10.1109/TNSRE.2019.2904924.
- 14. Sawicki, G.S.; Beck, O.N.; Kang, I.; Young, A.J. The Exoskeleton Expansion: Improving Walking and Running Economy. *J. Neuroeng. Rehabil.* 2020, *17*, 1–9, doi:10.1186/S12984-020-00663-9/TABLES/1.
- 15. Kim, J.; Quinlivan, B.T.; Deprey, L.A.; Arumukhom Revi, D.; Eckert-Erdheim, A.; Murphy, P.; Orzel, D.; Walsh, C.J. Reducing the Energy Cost of Walking with Low Assistance Levels through Optimized Hip Flexion Assistance from a Soft Exosuit. *Sci. Rep.* 2022, *12*, 1–13, doi:10.1038/s41598-022-14784-9.
- 16. Ding, Y.; Panizzolo, F.A.; Siviy, C.; Malcolm, P.; Galiana, I.; Holt, K.G.; Walsh, C.J. Effect of Timing of Hip Extension Assistance during Loaded Walking with a Soft Exosuit. *J. Neuroeng. Rehabil.* 2016, *13*, 87–87, doi:10.1186/S12984-016-0196-8.
- 17. Zhou, T.; Xiong, C.; Zhang, J.; Hu, D.; Chen, W.; Huang, X. Reducing the Metabolic Energy of Walking and Running Using an Unpowered Hip Exoskeleton. *J. Neuroeng. Rehabil.* 2021, *18*, 95, doi:10.1186/s12984-021-00893-5.

- 18. Browning, R.C.; Modica, J.R.; Kram, R.; Goswami, A. The Effects of Adding Mass to the Legs on the Energetics and Biomechanics of Walking. *Med. Sci. Sport. Exerc.* 2007, 39, 515–525, doi:10.1249/mss.0b013e31802b3562.
- 19. Dembia, C.L.; Silder, A.; Uchida, T.K.; Hicks, J.L.; Delp, S.L. Simulating Ideal Assistive Devices to Reduce the Metabolic Cost of Walking with Heavy Loads. *PLoS One* 2017, *12*, doi:10.1371/journal.pone.0180320.
- 20. Mooney, L.M.; Herr, H.M. Biomechanical Walking Mechanisms Underlying the Metabolic Reduction Caused by an Autonomous Exoskeleton. *J. Neuroeng. Rehabil.* 2016, *13*, 4, doi:10.1186/s12984-016-0111-3.
- 21. Roberts, D.; Hillstrom, H.; Kim, J.H. Instantaneous Metabolic Cost of Walking: Joint-Space Dynamic Model with Subject-Specific Heat Rate. *PLoS One* 2016, *11*, e0168070, doi:10.1371/journal.pone.0168070.
- 22. Umberger, B.R. Stance and Swing Phase Costs in Human Walking. *J. R. Soc. Interface* 2010, 7, 1329–1340, doi:10.1098/rsif.2010.0084.
- 23. Mohammadzadeh Gonabadi, A.; Antonellis, P.; Malcolm, P. Differences between Joint-Space and Musculoskeletal Estimations of Metabolic Rate Time Profiles. *PLOS Comput. Biol.* 2020, *16*, e1008280, doi:10.1371/journal.pcbi.1008280.
- 24. Lee, G.; Kim, J.; Panizzolo, F.A.; Zhou, Y.M.; Baker, L.M.; Galiana, I.; Malcolm, P.; Walsh, C.J. Reducing the Metabolic Cost of Running with a Tethered Soft Exosuit. *Sci. Robot* 2017, *2*, 6708–6731, doi:10.1126/scirobotics.aan6708.
- 25. Nasiri, R.; Ahmadi, A.; Ahmadabadi, M.N. Reducing the Energy Cost of Human Running Using an Unpowered Exoskeleton. *IEEE Trans. Neural Syst. Rehabil. Eng.* 2018, *PP*, 1, doi:10.1109/TNSRE.2018.2872889.
- 26. Kim, J.; Lee, G.; Heimgartner, R.; Arumukhom Revi, D.; Karavas, N.; Nathanson, D.; Galiana, I.; Eckert-Erdheim, A.; Murphy, P.; Perry, D.; et al. Reducing the Metabolic Rate of Walking and Running with a Versatile, Portable Exosuit. *Science* (80-.). 2019, 365, 668–672, doi:10.1126/science.aav7536.
- 27. Zhang, Y.; Ajoudani, A.; Tsagarakis, N.G. Exo-Muscle: A Semi-Rigid Assistive Device for the Knee. *IEEE Robot. Autom. Lett.* 2021, 6, 8514–8521, doi:10.1109/LRA.2021.3100609.
- 28. Schmidt, K.; Duarte, J.E.; Grimmer, M.; Sancho-Puchades, A.; Wei, H.; Easthope, C.S.; Riener, R. The Myosuit: Bi-Articular Anti-Gravity Exosuit That Reduces Hip Extensor Activity in Sitting Transfers. *Front. Neurorobot.* 2017, *11*, doi:10.3389/fnbot.2017.00057.
- 29. Lin, L.; Zhang, F.; Yang, L.; Fu, Y. Design and Modeling of a Hybrid Soft-Rigid Hand Exoskeleton for Poststroke Rehabilitation. *Int. J. Mech. Sci.* 2021, *212*, 106831, doi:10.1016/j.ijmecsci.2021.106831.
- 30. Caputo, J.M.; Collins, S.H. A Universal Ankle Foot Prosthesis Emulator for Human Locomotion Experiments. 2015, *136*, 1–10, doi:10.1115/1.4026225.
- 31. Simha, S.N.; Wong, J.D.; Selinger, J.C.; Donelan, J.M. A Mechatronic System for Studying Energy Optimization during Walking. *IEEE Trans. Neural Syst. Rehabil. Eng.* 2019, 1–1, doi:10.1109/tnsre.2019.2917424.
- 32. Gonabadi, A.M.; Antonellis, P.; Malcolm, P. A System for Simple Robotic Walking Assistance With Linear Impulses at the Center of Mass. *IEEE Trans. Neural Syst. Rehabil. Eng.* 2020, 28, 1353–1362, doi:10.1109/tnsre.2020.2988619.
- 33. Brockway, J. Derivation of Formulae Used to Calculate Energy Expenditure in Man. *Hum. Nutr. Clin. Nutr.* 1987, *41*, 463–471.
- 34. Zhang, J.; Fiers, P.; Witte, K.A.; Jackson, R.W.; Poggensee, K.L.; Atkeson, C.G.; Collins, S.H. Human-in-the-Loop Optimization of Exoskeleton Assistance during Walking. *Science* 2017, *356*, 1280–1284, doi:10.1126/science.aal5054.
- 35. Selinger, J.C.; Donelan, J.M. Estimating Instantaneous Energetic Cost during Non-Steady-State Gait. J. Appl.

- Physiol. 2014, 117, 1406-1415, doi:10.1152/japplphysiol.00445.2014.
- 36. Kadaba, M.P.; Ramakrishnan, H.K.; Wootten, M.E. Measurement of Lower Extremity Kinematics during Level Walking. *J. Orthop. Res.* 1990, *8*, 383–392, doi:10.1002/jor.1100080310.
- 37. Seth, A.; Hicks, J.L.; Uchida, T.K.; Habib, A.; Dembia, C.L.; Dunne, J.J.; Ong, C.F.; DeMers, M.S.; Rajagopal, A.; Millard, M.; et al. OpenSim: Simulating Musculoskeletal Dynamics and Neuromuscular Control to Study Human and Animal Movement. *PLoS Comput. Biol.* 2018, *14*, e1006223, doi:10.1371/journal.pcbi.1006223.
- 38. Delp, S.L.; Anderson, F.C.; Arnold, A.S.; Loan, P.; Habib, A.; John, C.T.; Guendelman, E.; Thelen, D.G. OpenSim: Open-Source Software to Create and Analyze Dynamic Simulations of Movement. *IEEE Trans. Biomed. Eng.* 2007, *54*, 1940–1950, doi:10.1109/TBME.2007.901024.
- 39. Hicks, J.L.; Uchida, T.K.; Seth, A.; Rajagopal, A.; Delp, S.L. Is My Model Good Enough? Best Practices for Verification and Validation of Musculoskeletal Models and Simulations of Movement. *J. Biomech. Eng.* 2015, *137*, doi:10.1115/1.4029304.
- 40. Donelan, J.M.; Kram, R.; Kuo, A.D. Simultaneous Positive and Negative External Mechanical Work in Human Walking. *J Biomech* 2002, *35*, 117–124.
- 41. John W. Tukey Exploratory Data Analysis; Pearson, 1977;
- 42. Pratt, G.A.; Williamson, M.M. Series Elastic Actuators. *IEEE Int. Conf. Intell. Robot. Syst.* 1995, *1*, 399–406, doi:10.1109/iros.1995.525827.
- 43. Vallery, H.; Veneman, J.; van Asseldonk, E.; Ekkelenkamp, R.; Buss, M.; van Der Kooij, H. Compliant Actuation of Rehabilitation Robots. *IEEE Robot. Autom. Mag.* 2008, *15*, 60–69, doi:10.1109/MRA.2008.927689.
- 44. Zhang, J.; Collins, S.H. The Passive Series Stiffness That Optimizes Torque Tracking for a Lower-Limb Exoskeleton in Human Walking. *Front. Neurorobot.* 2017, *11*, 1–16, doi:10.3389/fnbot.2017.00068.
- 45. Zhang, J.; Collins, S.H. The Passive Series Stiffness That Optimizes Torque Tracking for a Lower-Limb Exoskeleton in Human Walking. *Front. Neurorobot.* 2017, *11*, 263786, doi:10.3389/FNBOT.2017.00068/BIBTEX.
- 46. Lewis, C.L.; Ferris, D.P. Walking with Increased Ankle Pushoff Decreases Hip Muscle Moments. *J. Biomech.* 2008, *41*, 2082–2089, doi:10.1016/j.jbiomech.2008.05.013.
- 47. Ding, Y.; Kim, M.; Kuindersma, S.; Walsh, C.J. Human-in-the-Loop Optimization of Hip Assistance with a Soft Exosuit during Walking. *Sci. Robot.* 2018, 3, eaar5438, doi:10.1126/scirobotics.aar5438.
- 48. Antonellis, P.; Mohammadzadeh Gonabadi, A.; Myers, S.A.; Pipinos, I.I.; Malcolm, P. Metabolically Efficient Walking Assistance Using Optimized Timed Forces at the Waist. *Sci. Robot.* 2022, 7, doi:10.1126/scirobotics.abh1925.
- 49. Bryan, G.M.; Franks, P.W.; Song, S.; Reyes, R.; O'Donovan, M.P.; Gregorczyk, K.N.; Collins, S.H. Optimized Hip-Knee-Ankle Exoskeleton Assistance Reduces the Metabolic Cost of Walking with Worn Loads. *J. Neuroeng. Rehabil.* 2021, *18*, 161, doi:10.1186/s12984-021-00955-8.
- 50. Galle, S.; Malcolm, P.; Derave, W.; De Clercq, D. Adaptation to Walking with an Exoskeleton That Assists Ankle Extension. *Gait Posture* 2013, *38*, 495–499, doi:10.1016/j.gaitpost.2013.01.029.